Peer-reviewed version available at *Minerals* **2018**, *8*, 519; doi:10.3390/min8110519

Technical Note

Critical Metal Particles in Copper Sulfides from the Supergiant Río Blanco Porphyry Cu-Mo Deposit, Chile

Jorge Crespo [1,*], Martin Reich [1], Fernando Barra [1], Juan José Verdugo [2] and Claudio Martínez [2]

[1] Department of Geology and Andean Geothermal Center of Excellence (CEGA), FCFM, Universidad de Chile, Plaza Ercilla 803, Santiago, Chile; mreich@ing.uchile.cl (M.R.); fbarrapantoja@ing.uchile.cl (F.B.)
[2] CODELCO, División Andina, Avenida Santa Teresa, N° 513 Los Andes, V Región, Chile; jverdugo@codelco.cl (J.J.V); cmart006@codelco.cl (C.M.)
* Correspondence: jorge.crespo@ug.uchile.cl (J.C.); Tel.: +56-9-89783139

Abstract: Porphyry copper-molybdenum deposits (PCDs) are the world's most important source of copper, molybdenum and rhenium. Previous studies have reported that some PCDs can have sub-economic to economic grades of critical metals, i.e., those elements that are both essential for modern societies and subject to the risk of supply restriction (e.g., platinum group elements (PGE), rare earth elements (REE), In, Co, Te, Ge, Ga, among others). Even though some studies have reported measured concentrations of Pd and Pt in PCDs, their occurrence and mineralogical form remain poorly constrained. Furthermore, these reconnaissance studies have focused predominantly on porphyry Cu-Au deposits, but very limited information is available for porphyry Cu-Mo systems. In this contribution, we report the occurrence of critical metal (Pd, Pt, Au, Ag, and Te) inclusions in copper sulfides from one of the most world's largest PCD, the supergiant Río Blanco-Los Bronces deposit in central Chile. Field emission scanning electron microscope (FESEM) observations of chalcopyrite and bornite from the potassic alteration zone reveal the presence of micro- to nano-sized particles (<1-10 μm) of noble metals, most notably Pd, Au, and Ag. The mineralogical data show that these inclusions are mostly tellurides, such as merenskyite [$PdTe_2$], Pd-rich hessite [Ag_2Te], sylvanite [(Ag, Au)Te_2] and petzite [Ag_3AuTe_2]. The data point to Pd (and probably Pt) partitioning in copper sulfides during the high-temperature potassic alteration stage, opening new avenues of research aimed at investigating not only the mobility of PGE during mineralization and partitioning into sulfides, but also at evaluating the potential of porphyry Cu-Mo deposits as a source for noble metals.

Keywords: platinum-group elements, silver, gold, Pd-tellurides, porphyry Cu-Mo, Rio Blanco –Los Bronces, Chile.

---

1. Introduction

Porphyry Cu-Mo deposits (PCDs) are typically associated with calc-alkaline intrusive rocks and currently provide 60% of world's copper supply [1]. In addition to copper, PCDs are major sources of molybdenum and rhenium [2], and previous studies have reported the presence of relevant amounts of other metals including Au, Ag, Se, Te, U, W, Bi, Co, and platinum group elements (PGE) [3-11]. Some of these elements are considered "critical" for the expected growth of technology and renewable energy resources and thus, are both essential for modern societies and subject to the risk of supply restriction [12-14]. Despite their strategic importance, surprisingly few trace element concentration data are available for sulfides in PCDs when compared to other deposits such as orogenic, epithermal, Carlin-type Au deposits, and volcanogenic massive sulfide (VMS) deposits [15-18]. Only a small number of studies have constrained the concentrations of trace metals in ore and gangue sulfides from PCDs using modern micro-analytical

Peer-reviewed version available at Minerals 2018, 8, 519; doi:10.3390/min8110519

techniques (e.g., [7, 19 – 23]; hence, many questions still remain concerning the speciation and mineralogical form of trace metals within sulfides.

Among trace metals, gold and silver are relevant byproducts in porphyry Cu-Mo deposits, with estimated median grades of 9 ppb Au and ~1 ppm Ag [24]. Previous studies have shown that Au is preferentially incorporated into bornite and chalcopyrite within potassic alteration zones, with concentrations reaching ~2-4 ppm in chalcopyrite and ~80-364 ppm in bornite [7, 25]. Silver, on the other hand, has been reported to reach up to 100's to 1000's ppm in bornite, chalcopyrite and chalcocite in porphyry-type deposits in northern Chile [26, 27]. A recent study in PCDs from Romania shows that Ag in bornite is an order of magnitude greater than in chalcopyrite, and two orders of magnitude higher than in pyrite [20].

Anomalous PGE concentrations have been documented in a number of PCDs worldwide. Tarkian et al., 1999 [4] reported PGE data from sulfide and flotation concentrates from thirty-three PCDs from Chile, Peru, Argentina, US, Canada, Indonesia and Papua New Guinea. The cited study reveals that PCDs can contain relatively high Pd concentrations (130–1900 ppb) that are correlated with high Au contents (1–28 ppm). Tarkian et al., 1999 [4] also identified the presence of platinum group minerals (PGM), which occurred as micrometer-scale inclusions in chalcopyrite. Pašava et al., 2010 [9] reported an average Pd value of 55.2 ppb in flotation concentrates from the Kalmakyr porphyry Cu-Au-Mo deposit in Uzbekistan and where the concentration of Pd and Au show a strong correspondence with copper. Palladium was also found associated with Ag, Se, and S in two alkalic porphyry Cu-Au deposits (the Afton and Mount Milligan deposits) in the Canadian Cordillera [28]. The cited authors documented that at least 90% of the bulk Pd+Pt occurs within pyrite and not related to copper sulfides. Both Pd and Pt are highly enriched in the cores of the pyrite grains (up to 90 ppm and 20 ppm, respectively) and their abundance correlates well with the Co content in pyrite (up to 4 wt%). These large concentrations of trace metals have not been observed directly in porphyry Cu-Mo deposits, an attribute that has led to overlooking their PGE potential.

Here, we document the occurrence of noble metal (Au, Ag, and Pd)-bearing mineral inclusions in copper sulfides within the potassic alteration zone of the world-class Río Blanco porphyry Cu-Mo deposit in central Chile. We combined observations using field emission scanning electron microscopy (FESEM) and electron microprobe analyses (EMPA) of selected grains of chalcopyrite and bornite. Our results show that PGE minerals may be more frequent in PCDs than previously thought, and that high-resolution FESEM techniques greatly facilitate the imaging and characterization of micrometer to nanometer-sized particles in copper sulfides.

2. Geology of the Río Blanco deposit

The Río Blanco PCD is located ~60 km northeast of Santiago, at an altitude between 3700 and 4300 m above sea level in the high Andes of Central Chile (Fig. 1A). From north to south, mining activities are focused on three areas, i.e., the Río Blanco (RB) underground mine, and the Don Luis (DL) and Sur-Sur (SS) open pits (Fig. 1B). In 2017, the mine produced 220.000 tons of fine copper.

Preprints (www.preprints.org) | NOT PEER-REVIEWED | Posted: 15 October 2018 doi:10.20944/preprints201810.0322.v1

Peer-reviewed version available at Minerals 2018, 8, 519; doi:10.3390/min8110519

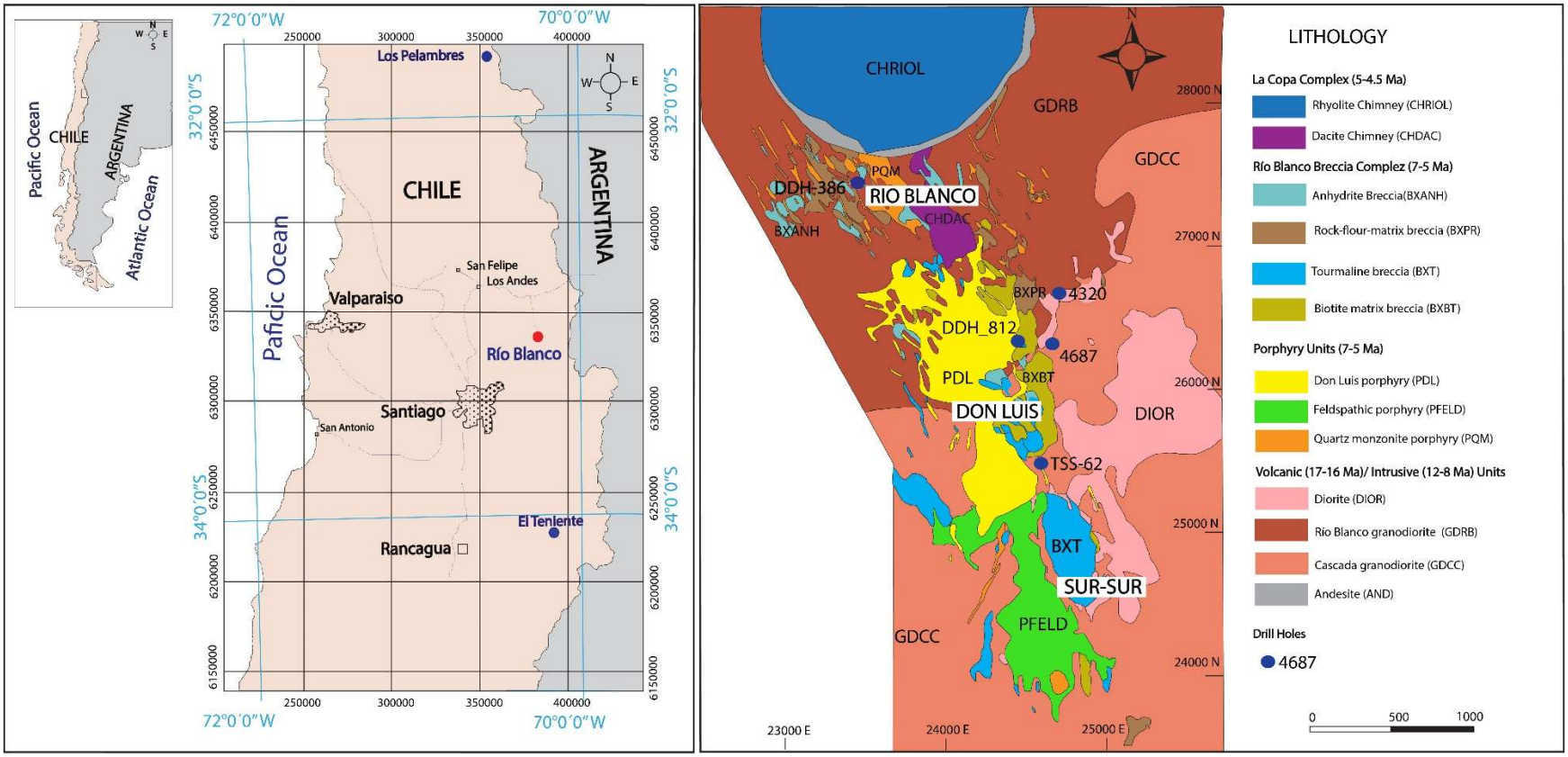

(A) (B)

Figure 1. (A) Location of the Río Blanco porphyry Cu-Mo deposit in Central Chile. The location of other major PCDs are also shown. **(B)** Geology of the Río Blanco PCD, modified after Ferraz and Cruz (2011)

Peer-reviewed version available at Minerals 2018, 8, 519; doi:10.3390/min8110519

The oldest rocks in the Río Blanco PCD correspond to andesite lavas and stratified basaltic andesites of the Farellones Formation [29], with reported U-Pb zircon ages of 17.2 ± 0.05 Ma [30] (Fig. 1B). The Farellones Formation is intruded by the San Francisco Batholith (SFB), which comprises granodiorites, monzodiorites, and tonalites [31, 32]. The SFB comprises several magmatic pulses, including the Río Blanco granodiorite (GDRB) and the Cascada granodiorite (GDCC), with reported U-Pb zircon ages of 11.96 ± 0.04 Ma and 8.4 ± 0.23 Ma, respectively [30].

The SFB is cut by porphyries of quartz monzonitic (PQM) and feldspathic (PFELD) compositions, with reported U-Pb zircon ages of 6.32 ± 0.09 Ma and 5.84 ± 0.03 Ma, respectively [30] (Fig. 1B). Several hydrothermal breccia types are recognized in Río Blanco: igneous, igneous/hydrothermal, hydrothermal (biotite and tourmaline bearing), and rock-flour breccias [33]. The hydrothermal breccias are closely related to the porphyry units and the bulk of the copper sulfide mineralization occurs as cement in these breccias. The Don Luis porphyry (PDL) crosscuts the mineralized breccia complex and corresponds to a subvertical intrusion of dacitic composition (U-Pb zircon age of 5.23 ± 0.07 Ma [30]). The youngest unit in the district corresponds to the La Copa Volcanic Complex (CVLC), which is located in the northern part of the deposit. The CVLC comprises crystalline tuffs (CHDAC, Dacitic chimney; U-Pb zircon age of 4.57 ± 0.08 Ma) and lithic tuffs (CHRIOL, Rhyolitic chimney; U-Pb zircon age of 4.31 ± 0.05 Ma) [33]). Magmatic and hydrothermal fluid flow was channeled and focused by both sets of preexisting oblique structures (NE and NW –striking faults) and, in turn, fault rupture was driven by high fluid pressures [34].

Hydrothermal alteration at the Río Blanco PCD is characterized by a propylitic (chlorite-epidote) alteration that grades to biotite-chlorite and biotite towards the innermost part of the deposit (CODELCO-technical report 2014). Potassic alteration is related to the porphyry phases, and is characterized by a high content of biotite + potassium feldspar ± albite and lower contents of anhydrite. Potassic alteration occurs at depth, with chalcopyrite ± bornite ± molybdenite and minor pyrite. This early alteration is identified by three types of veinlets: (i) EBT veins characterized by quartz + chalcopyrite ± bornite ± K feldspar ± anhydrite with biotite haloes, (ii) sinuous, type-A veinlets with quartz ± K feldspar ± chalcopyrite, and (iii) thicker, B-type veinlets with quartz ± molybdenite (CODELCO-technical report 2014). The phyllic stage, overimposed on the potassic alteration event, is defined by the development of C-type veinlets gray-green sericite (GGS) with quartz + chalcopyrite, and a halo with phengite-celadonite ± K feldspar and abundant chalcopyrite ± bornite ± pyrite. This GGS alteration varies from strong to moderate to weak from the center to the outer zones of the deposit. In the shallowest parts of the deposit, a late-stage alteration event is recognized by the presence of D-type quartz-sericite veinlets (QS), composed of quartz + pyrite ± chalcopyrite and sericite ± clays (illite-kaolinite) halos with pyrite>chalcopyrite [35]. Late E-type veinlets are composed of quartz + carbonates (siderite-ankerite) + pyrite ± gypsum ± sphalerite ± tennantite ± enargite-luzonite ± galena ± bornite, with a sericite + clays halo.

3. Samples and Methods

CODELCO-Andina has a multi-element (51 elements) ICP-MS geochemical database of 10140 samples (whole rock) from drill holes. A total of twenty-eight core-samples from six drill holes that cross-cut the main mineralization-alteration zones at the Río Blanco deposit were collected for this study. The samples were selected based on their Ag, Bi, and Te contents, with a focus on high grade material (> 3 ppm Ag, 1.32 ppm Bi, and 0.24 ppm Te). The sulfide minerals studied here included chalcopyrite and bornite from the potassic alteration zone. Polished thick sections were inspected for the presence of micro- to nano-meter sized inclusions using a combination of conventional and field-emission scanning electron microscopy techniques. The SEM observations were carried out at the Andean Geothermal Center of Excellence (CEGA), Universidad de Chile, using a FEI Quanta 250 SEM equipped with a secondary electron (SE) and backscattered electron (BSE) detectors, and an energy-dispersive X-ray spectrometer (EDS). The analytical parameters were: accelerating voltage of 15-20 kV and an emission current of ~80 μA, takeoff angle ~35°,

spot beam was 4-5 μm in diameter, and a working distance of ~10 mm. Semi-quantitative EDS analyses were used to identify major elements in individual mineral phases. High-resolution imaging of micro- to nano-sized inclusions was achieved using field-emission scanning electron microscopy (FESEM). Observations were performed using a FEI Quanta 250 FEG at the Center for Research in Nanotechnology and Advanced Materials (CIEN) at the Pontificia Universidad Católica de Chile, Santiago, Chile. The FESEM is equipped with in-column detector (ICD) for SE and BSE, and an EDS detector. Operating conditions included an accelerating voltage of 20 kV, spot beam was ~4 μm in diameter, takeoff angle ~35-37°, live time was 45 s and a working distance of ~10 mm.

In addition, major and minor element contents in chalcopyrite and bornite, and one palladium telluride inclusion were determined by electron microprobe analysis (EMPA) using a JEOL JXA-8230 Superprobe at the LAMARX Laboratory of the Universidad Nacional de Córdoba, Argentina. Elements and X-ray lines used for the analysis were Hg (Mα), Te (Lα), Se (Lα), Bi (Mα), Au (Mα), S (Kα), Fe (Kα), Co (Kα), Zn (Kα), As (Kα), Ag (Lα), Pb (Mβ), Sb (Lα), Cu (Kα), Ni (Kα), Mn (Kα), Pt (Mα), Re (Mα), Pd (Lα), Rh (Lα), Ru (Lα), Ir (Mα), Os (Mα). Operating conditions included an accelerating voltage of 20 kV and beam current of 20 nA, and the electron beam was ~1 μm in diameter. Counting time was 40 s for Hg, Te, Se, Bi, Au, S, Fe, Co, Zn, As, Ag, Pb, Sb, Cu, Ni, and Mn. Counting time was 20 s for Pt, Re, Pd, Rh, Ru, Ir, and Os. Standard specimens used for calibration were HgTe (for Hg and Te), NiSe (for Ni and Se), Bi_2S_3 (for Bi), Au (for Au), $CuFeS_2$ (for Cu, Fe and S), $CoAs_3$ (for Co), ZnS (for Zn), NiAs (for As), Ag^0 (for Ag), PbS (for Pb), Sb_2S_3 (for Sb), Mn^0 (for Mn), Pt^0 (for Pt), Re^0 (for Re), Pd^0 (for Pd), Rh^0 (for Rh), Ru^0 (for Ru), Ir^0 (for Ir) and Os^0 (for Os).

4. Results

EMPA analyses reveal that chalcopyrite and bornite contain significant amounts of Ag (<1400 ppm), Au (<800 ppm), Co (<600 ppm) and Te (<300 ppm). Other minor elements detected include As (<1300 ppm), Hg (<1200 ppm), Pb (<700 ppm), Bi (<700 ppm), Se (<300 ppm), and Ni (<100 ppm) (Table 1).

Table 1. The summary of the EMPA representative analyses of chalcopyrite and bornite from Rio Blanco deposit in (wt %).

Sample	Cu	Fe	S	Au	Ag	Bi	Hg	Te	Se	Zn	As	Pb	Sb	Co	Ni	Total
	0.01	0.01	0.01	0.02	0.01	0.03	0.03	0.01	0.01	0.01	0.02	0.02	0.01	0.02	0.01	
DDH386-564																
C1-Cpy2	35.32	29.10	34.11	b.d	b.d	b.d	0.10	0.03	b.d	b.d	0.02	0.05	b.d	b.d	b.d	98.78
C1-Cpy3	35.17	29.42	34.09	b.d	b.d	b.d	b.d	0.03	b.d	b.d	b.d	0.03	b.d	0.04	b.d	98.78
C4-Cpy10	35.24	29.43	34.33	b.d	b.d	0.06	b.d	b.d	b.d	b.d	b.d	b.d	b.d	b.d	b.d	99.07
C4-Cpy11	35.31	29.32	34.26	0.08	b.d	b.d	b.d	b.d	0.02	b.d	b.d	b.d	b.d	0.04	0.01	99.05
C4-Cpy12	35.38	29.42	34.46	b.d	b.d	b.d	0.12	b.d	0.02	b.d	b.d	0.07	b.d	b.d	b.d	99.49
C3-Cpy13	35.55	29.88	34.26	b.d	0.04	0.07	0.03	0.02	0.03	b.d	0.03	0.03	b.d	0.06	b.d	100.00
C3-Cpy14	35.69	29.84	34.38	b.d	b.d	0.05	0.09	b.d	0.02	b.d	0.06	0.04	b.d	0.02	b.d	100.19
C4-Bn8	63.85	10.99	25.55	b.d	0.14	b.d	0.10	b.d	b.d	b.d	b.d	b.d	b.d	0.02	b.d	100.65
C4-Bn9	63.90	11.09	25.48	b.d	0.13	b.d	0.05	0.03	b.d	b.d	0.04	b.d	b.d	b.d	b.d	100.74
C3-Bn15	62.67	11.62	25.76	b.d	0.04	0.06	b.d	b.d	b.d	b.d	0.08	0.07	b.d	b.d	b.d	100.30
C3-Bn16	62.88	11.27	25.93	b.d	0.06	b.d	0.09	b.d	0.02	b.d	0.13	b.d	b.d	0.02	0.01	100.42
C3-Bn17	62.47	11.28	26.02	0.05	0.06	0.07	0.10	b.d	b.d	b.d	0.12	b.d	b.d	0.02	b.d	100.22

Sample	Cu	Fe	S	Au	Ag	Bi	Te	Pd	Pt	Re	As	Rh	Ru	Ir	Os	Ni	Total
	0.01	0.01	0.01	0.02	0.01	0.06	0.03	0.03	0.04	0.03	0.02	0.02	0.02	0.03	0.03	0.02	
DDH386-564																	
C4-PdTe8	2.75	1.83	1.56	0.13	b.d	0.35	65.34	23.69	1.32	b.d	b.d	b.d	b.d	b.d	0.12	b.d	97.11

Notes: b.d = below detection limits; detection limits (wt%) are shown below each element.

Preprints (www.preprints.org) | NOT PEER-REVIEWED | Posted: 15 October 2018 doi:10.20944/preprints201810.0322.v1

Peer-reviewed version available at Minerals 2018, 8, 519; doi:10.3390/min8110519

Detailed FESEM inspection of Ag-bearing chalcopyrite and bornite grains revealed the presence of micrometer to nanometer-sized mineral inclusions (Figs. 2 and 3).

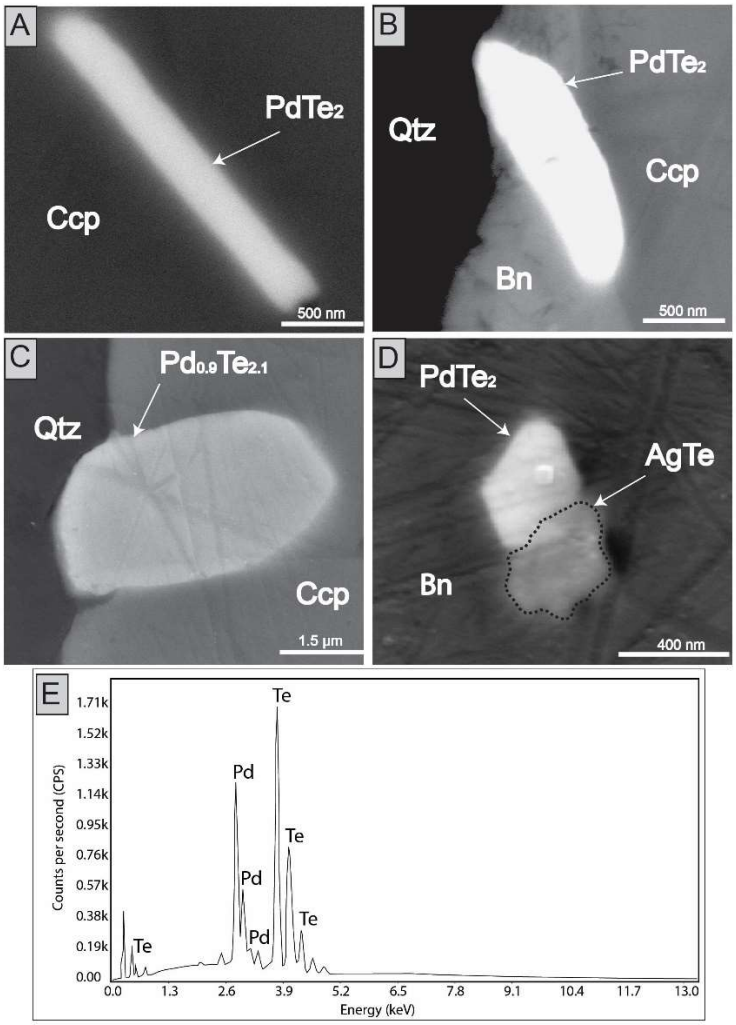

Figure 2. Field-emission scanning electron microscopy (FESEM) images of platinum group minerals (PGMs) in chalcopyrite and bornite from Río Blanco. Palladium tellurides are shown in images A, B, C, and D. Images A and B were taken using the back-scattered electron detector (BSE), while images C and D were taken using the secondary electron (SE) detector. Image E shows the EDS spectrum of the Pd telluride grain in image C. Ccp: chalcopyrite, Bn: bornite, Qtz: quartz, AgTe: silver telluride, $PdTe_2$: merenskyite.

The inclusions occur usually along grain boundaries (Fig. 2B) and their morphology varies from subhedral to tabular, with sizes ranging from ~400 nm to ~4 µm. Due to the sub-micrometer size of most inclusions, chemical characterization was carried out semi-quantitatively by means of FESEM-EDS. In most grains, Pd and Te were detected along with Cu, Fe, and S from the sulfide host matrix (Fig. 2A, 2B and 2D). One quantitative EMPA-WDS spot analysis of a micrometer-sized inclusion (Fig. 2C) shows ~23.7 wt% Pd and 65.3 wt% Te (Table 1). Despite the low total (~97 wt%), the stoichiometry is consistent with the mineral merenskyite [$PdTe_2$]. EMPA-WDS analysis of the same grain (Fig. 2C) indicates the presence of Pt (1.3 wt%), Au (0.1 wt%), Os (0.1 wt%) and Bi (0.4 wt%). FESEM-EDS analyses of the other Pd-Te-bearing grains shown in Figure 2 are broadly consistent with merenskyite.

Mineral inclusions containing Au, Ag, Hg, and Te are shown in Figure 3. Most of these inclusions have anhedral to subhedral forms, some with rectangular and tabular/elongated shapes, and occur along grain

Preprints (www.preprints.org) | NOT PEER-REVIEWED | Posted: 15 October 2018 doi:10.20944/preprints201810.0322.v1

Peer-reviewed version available at Minerals 2018, 8, 519; doi:10.3390/min8110519

boundaries (Fig. 3A). Semi-quantitative FESEM-EDS analysis indicate that the inclusions are most likely electrum [Au, Ag±Hg] (Fig. 3A-D), and Au-Ag-Te minerals such as petzite [Au_3AgTe_2] (Fig. 3B).

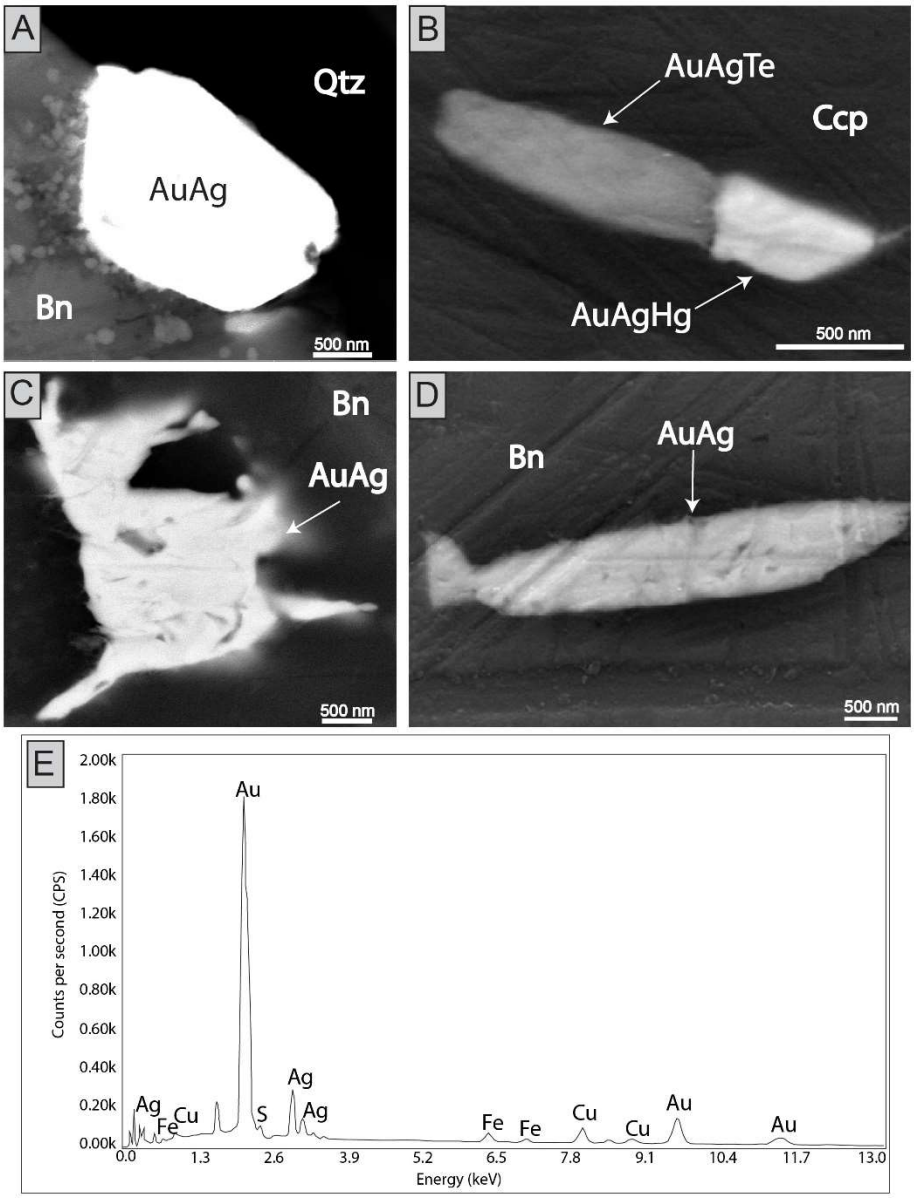

Figure 3. Field-emission scanning electron microscopy (FESEM) images of silver, gold, mercury, and tellurium mineral inclusions in chalcopyrite and bornite from Río Blanco. Electrum (Au,Ag) grains are shown images A, B, C, and D. Au-Ag-Te and Au-Ag-Hg phases are shown in B. Images A and C were taken using the back-scattered electron (BSE) detector, while images B and D were taken the secondary electron (SE) detector. Image E shows the EDS spectrum of the electrum grain shown in A. Ccp: chalcopyrite, Bn: bornite, Qtz: quartz, AuAg: electrum, AuAgTe: possibly sylvanite or petzite.

5. Discussion

Anomalous PGE contents were previously reported in Cu-Fe sulfides and flotation concentrates from several porphyry Cu-Au deposits [4], where high Pd contents (130-1900 ppb) are associated with high Au

Preprints (www.preprints.org) | NOT PEER-REVIEWED | Posted: 15 October 2018 doi:10.20944/preprints201810.0322.v1

Peer-reviewed version available at Minerals 2018, 8, 519; doi:10.3390/min8110519

contents (1-28 ppm). Additionally, Pašava et al., 2010 [9] showed in the Kalmarkyr porphyry Cu-Au-Mo deposit in Uzbekistan average concentrations of 55 ppb Pd, 5.5 ppb Pt, and 4.1 ppm Au for disseminated and stockwork-type high-grade Cu-Au-Mo mineralization. Economou-Eliopoulos et al., 2000 [5] reported relatively high Pd contents in the Skouries PCD in Greece, ranging between 60 and 200 ppb (average 110 ppb). Furthermore, Economou-Eliopoulos 2005 [8] concluded that PGE-bearing porphyries have similar characteristics, including: a) Their association with alkaline or K-rich calc-alkaline systems; b) The dominant occurrence of Pd-bearing minerals (merenskyite) within Cu sulfides, in association with Au-Ag tellurides, and c) The association of Pd, Pt, and Au with magnetite-bornite-chalcopyrite assemblages, within the pervasive potassic alteration zones in the central parts of the deposits.

The features described above are broadly similar to the occurrences of PGM in the Río Blanco PCD, reported in this technical note. Our observations indicate that Pd, Pt, Au, Ag, and Te form micrometer to nanometer-sized mineral inclusions within chalcopyrite and bornite (Figs. 2 and 3). The PGM, Au, and Ag were found in early EBT veins characterized by quartz + chalcopyrite ± bornite ± K feldspar ± anhydrite with biotite haloes, and in type-A veinlets with quartz ± K feldspar ± chalcopyrite, which are characteristic veins of the penetrative potassium feldspar alteration zone. Gold is found as electrum (Au, Ag), whereas the most common silver-bearing mineral is hessite, which was observed intergrown with merenskyite ($PdTe_2$-Ag_2Te). It is relevant to mention that Tarkian et al., 1999 [4] analyzed mineral concentrates from the major Chilean porphyry Cu-Mo deposits, i.e., Río Blanco, Chuquicamata, Escondida, El Salvador and El Teniente. Among these deposits, only in Río Blanco the cited authors did not report detectable Pd and Pt concentrations. Since the aforementioned study focused on flotation concentrates and no information was provided about the provenance of the samples within the deposit, it is likely that the apparent lack of Pd and Pt at Río Blanco was related to the fact that at the time, CODELCO was not mining the (deeper) potassic alteration zone and the studied concentrate came from the upper portions of the deposit.

The mineralogical occurrence of Pd-bearing minerals (e.g., merenskyite, $PdTe_2$) at Río Blanco indicates that Pd was most likely introduced during the early potassic alteration stage. Xiong et al., 2000 [36] conducted a series of experiments on the solubility of Pd under hydrothermal conditions. High temperature, oxidized and highly saline fluid conditions are thought to favor the hydrothermal transport of PGEs. Xiong et al., 2000 [36] concluded that in the earlier stages of porphyry Cu-Mo formation, fluids are fully capable of transporting at least 10 ppb Pd. Recent experiments by Sullivan et al., 2018 [37] showed that Pd solubility increase with fO_2, indicating that Pd is dissolved in the silicate melt at ΔNNO between 0 and +1. Although the addition of Cl has a negligible effect on the solubility of Pd, experimental studies have shown that $PdCl^{-}_{4}$ predominates between 25 and 300 °C. This complex is the main species at the Cl^- concentrations observed in most hydrothermal fluids [38]. Since chloride ligands are generally invoked for Cu and Au transport in the porphyry environment [39, 40], the close association of Cu-sulfides and noble metal (Au-Pd-Ag) inclusions at Río Blanco may be explained, in part, by a similar transport and deposition mechanism as their host minerals. An alternative mechanism of PGE enrichment may involve Pd-Bi-Te phases, which may remain molten above 489ºC [41]. The aforementioned authors provide evidence of high Pd and Bi concentrations in brine inclusions from the Skouries PCD in Greece, suggesting that Bi-Te melts may act as a collectors for PGEs in high temperature hydrothermal fluids.

6. Concluding Remarks

The occurrence of Pd, Pt, and Au-bearing minerals in copper sulfides from the world-class Río Blanco deposit opens new avenues of research aimed at assessing the potential for PGE recovery. Also, the presence of PGE-bearing minerals in the potassic alteration zone at Río Blanco poses questions that are relevant to the understanding of the speciation and solubility of noble metals during mineralization and hydrothermal alteration. An equally important question is the quantity and intensity of the mineralizing (hydrothermal) events that contributed to the deposition of the noble metals in PCDs. These questions are closely linked

because the deposition of precious metals during different hydrothermal events could result in different incorporation forms into sulfides, i.e., solid solution *vs*. micro or nano-inclusions. Therefore, further micro-analytical studies are needed to address these questions, and to evaluate the sulfide phases formed under different physical and chemical conditions as hosts of PGEs and other strategic elements in porphyry Cu-Mo deposits.

Author Contributions: J.C. collected the samples and studied the sulfides using SEM, FESEM, and EMPA. All authors (J.C., M.R., F.B., J.J.V., and C.M.) discussed the results and evaluated the data. J.C., M.R. and F.B. wrote and organized the paper. J.J.V and C.M. provided geological information and granted access to the mine and drillcore libraries.

Funding: The work was supported by the Iniciativa Científica Milenio, which provided funding through grant #NC 130065 "Millennium Nucleus for Metal Tracing Along Subduction". Additional support was provided by the Andean Geothermal Center of Excellence (CEGA), FONDAP project #15090013. The Center for Research in Nanotechnology and Advanced Materials (CIEN) of the Pontifical Catholic University of Chile provided access to the FESEM used in this study, which was funded by FONDEQUIP Project EQM150101.

Acknowledgments: We thank the CODELCO Tech for providing a pre-doctoral Ph.D. scholarship to J. Crespo. The LAMARX Laboratory of the Universidad Nacional de Córdoba, Argentina, is acknowledged for granting access to the electron microprobe facility. This manuscript is dedicated to Romina, Naomi, and Tania.

Conflicts of Interest: The author declare no conflict of interest

References

1 Johnson K.M.; Hammarstrom J.M.; Zientek M. L.; Dicken C.L. Estimate of Undiscovered Copper Resources of the World, 2013. *US Geological Survey*. **2014**. http://dx.doi.org/10.3133/FS20143004

2 US Geological Survey. **2018**. Mineral Commodity Summaries 2018: U.S. Geological Survey, 200p., https://doi.org/10.3133/70194932

3 Einaudi M.T; Burt D.M. A Special Issue Devoted to Skarn Deposits. Introduction-Terminology, Classification, and Composition of Skarn Deposits. *Econ Geol.* **1982**, *77(4)*: 745–754. DOI: 10.2113/gsecongeo.77.4.745

4 Tarkian M.; Stribrny B. Platinum-group elements in porphyry copper deposits : a reconnaissance study. *Miner Petrol.* **1999**. *65*: 161–183. DOI: 10.1007/bf01161959

5 Economou-Eliopoulos M.; Eliopoulos D.G. Palladium, platinum and gold concentration in porphyry copper systems of Greece and their genetic significance. *Ore Geol Rev*. **1999**, *16*: 59–70. DOI: 10.1016/S0169-1368(99)00024-4

6 Simon G.; Kesler S.E; Essene E.J. Gold in Porphyry Copper Deposits: Experimental Determination of the Distribution of Gold in the Cu-Fe-S System at 400° to 700°C. *Econ Geol.* **2000**. *95(2)*: 259–270. DOI: 10.2113/gsecongeo.95.2.259

7 Kesler S.E.; Chryssoulis S.L.; Simon G. Gold in porphyry copper deposits: its abundance and fate. *Ore Geol Rev*. **2002.** *21*: 103–124. https://doi.org./10.1016/S0169-1368(02)00084-7

8 Economou-Eliopoulos M. Platinum-Group Element Potential of Porphyry Deposits. *Mineral Assoc Canada Short Course*. **2005**. *35*: 203–245

9 Pašava J.; Vymazalova A.; Kosler J.; Koneev R.; Jukov A.V.; Khalmatov R.A. Platinum-group elements in ores from the Kalmakyr porphyry Cu-Au-Mo deposit, Uzbekistan: bulk geochemical and laser

ablation ICP-MS data. *Miner Deposita*. **2010.** *45:* 411–418. https://doi.org/10.1007/s00126-010-0286-7

10 McFall K.A.; Roberts S.; Teagle D.; Naden J.; Lusty P.; Boyce A. The origin and distribution of critical metals (Pd, Pt, Te and Se) within the Skouries Cu-Au porphyry deposit, Greece. *Appl Earth Sci*. **2016.** 125(2): 100-1001

11 McFall K.A.; Naden J.; Roberts S.; Baker T.; Spratt J.; McDonald I. Platinum-group minerals in the Skouries Cu-Au (Pd, Pt, Te) porphyry deposit. *Ore Geol Rev*. **2018.** 99: 344-364. https://doi.org/10.106/j.oregeorev.2018.06.014

12 U.S. Departament Of Energy. Critical Materials Strategy, December 2011. Available online: https://www.energy.gov/sites/prod/files/DOE_CMS2011_FINAL_Full.pdf (accessed on 10 june 2018).

13 Geological Society of America. GSA Position Statement 2013 Critical Mineral and Materials. Available online: http://www.geosociety.org/gsa/positions/position23.aspx (accessed on 20 june 2018)

14 Arndt N.T.; Fontboté L.; Hedenquist J.W.; Kesler S.E.; Thompson J. F.H.; Wood D.G. Future Global Mineral Resources. *Geochem Perspect*. **2017.** 6: 1-171. DOI: 10.7185/geochempersp.6.1

15 Huston D.L.; Sie S.H.; Suter G.F.; Cooke D.R.; Both R.A. Trace Elements in Sulfide Minerals from Eastern Australian Volcanic-Hosted Massive Sulfide Deposits: Part I. Proton Microprobe Analyses of Pyrite, Chalcopyrite, and Sphalerite, and Part II. Selenium Levels in Pyrite: Comparison with (δ34S Values and Impli. *Econ Geol* **1995**. 90(5): 1167–1196. https://doi.org/10.2113/gsecongeo.90.5.1167

16 Kesler S.E.; Russell N.; Mccurdy K. Trace-metal content of the Pueblo Viejo precious-metal deposits and their relation to other high-sulfidation epithermal systems. *Miner Deposita* **2003** 38: 668–682. DOI: 10.1007/s00126-003-0356-1

17 Large R.R.; Danyushevsky L.; Hollit C.; Maslennikov V.; Meffre S.; Gilbert S.; Bull S.; Scott R.; Emsbo P.; Thomas H.; Singh B.; Foster J. Gold and Trace Element Zonation in Pyrite Using a Laser Imaging Technique: Implications for the Timing of Gold in Orogenic and Carlin-Style Sediment-Hosted Deposits. *Econ Geol* 2009. *104*: 635–668. DOI: 10.2113/gsecongeo.104.5.635

18 Deditius A.P.; Utsunomiya S.; Reich M.; Kesler S.E.; Ewing R.C.; Hough R.; Walshe J. Trace metal nanoparticles in pyrite. *Ore Geol Rev,* **2011**, 42: 32–46. https://doi.org/10.1016/j.oregeorev.2011.03.003

19 Reich M.; Deditius A.; Chryssoulis S.; Li J-W; Ma C-Q; Parada M.A.; Barra F.; Mittermayr F. Pyrite as a record of hydrothermal fluid evolution in a porphyry copper system: A SIMS/EMPA trace element study. *Geochim Cosmochim Ac*, **2013a,** 104: 42–62. https://doi.org/10.1016/j.gca.2012.11.006

20 Cioacă M.E.; Munteanu M.; Qi L.; Costin G. (2014) Trace element concentrations in porphyry copper deposits from Metaliferi Mountains, Romania: A reconnaissance study. *Ore Geol Rev,* **2014**, *63*: 22–39. https://doi.org/10.1016/j.oregeorev.2014.04.016

21 Franchini M.; Mcfarlane C.; Maydagán L.; Reich M.; Lentz D.R.; Meinert L.; Bouhier V. Trace metals in pyrite and marcasite from the Agua Rica porphyry-high sulfidation epithermal deposit, Catamarca, Argentina: Textural features and metal zoning at the porphyry to epithermal transition. *Ore Geol Rev*, **2015**, *66*: 366–387. https.77doi.org/10.1016/j.oregeorev.2014.10.022

22 Barra F.; Deditius A.; Reich M.; Kilburn M.; Guagliardo P.; Roberts M.P. Dissecting the Re-Os molybdenite geochronometer. *SCI REP-UK* **2017**, 7: 16054. DOI: 10.1038/s41598-017-16380-8

23 Zarasvandi A.; Rezaei M.; Raith J.G.; Pourkaseb H.; Asadi S.; Saed M.; Lentz D.R. Metal endowment reflected in chemical composition of silicates and sulfides of mineralized porphyry copper systems, Urumieh-Dokhtar magmatic arc, Iran. *Geochim Cosmochim Ac*, **2018**, *223*: 36–59. https://doi.org/10.1016/j.gca.2017.11.012

24 Singer D.A.; Berger V.I.; Moring B.C. Porphyry Copper Deposits of the World : Database And Grade and Tonnage models, 2008. U.S. Geological Survey, **2008**. Available online: https://pubs.usgs.gov/of/2008/1155/of2008-1155.pdf (accessed on 10 june 2018).

25 Sinclair W.D. Porphyry deposits, in Goodfellow W, ed., Mineral Deposits of Canada:. A synthesis of major Deposit-Types, District Metallogeny, the Evolution of Geological Provinces, and Exploration Methods: *Geological Association of Canada. Mineral Deposits Division. Special Publication* **2007**, 5: 223–243

26 Reich M.; Chryssoulis S.L.; Deditius A.; Palacios C.; Zuniga A.; Weldt M.; Alvear M. "Invisible" silver and gold in supergene digenite ($Cu_{1.8}S$). *Geochim Cosmochim Ac* **2010**,74: 6157-6173. https://doi.org/10.1016/j.gca.2010.07.026

27 Reich M.; Palacios C.; Barra F.; Chryssoulis S. "Invisible" silver in chalcopyrite and bornite from the Mantos Blancos Cu deposit, northern Chile. *Eur J Mineral* **2013b,** *25*: 453–460. DOI:10.1127/0935-1221/2013/0025-2287

28 Hanley J.J.; MacKenzie M. Incorporation of platinum-group elements and cobalt into subsidiary pyrite in alkalic Cu-Au porphyry deposits: significant implications for precious metal distribution in felsic magmatic-hydrothermal systems. *In AGU Spring Meeting Abstracts* **2009,** V14A-03.

29 Rivano S.; Godoy E.; Vergara M.; Villaroel R. Redefinición de la formacion farellones en la cordillera de los andes de chile central (32-34°S). *Rev Geol Chile* 1990, *17*: 205–214

30 Deckart K.; Clark A.H.; Aguilar A.C.; Vargas R.R.; Bertens A.N.; Mortensen J.K.; Fanning M. Magmatic and Hydrothermal Chronology of the Giant Río Blanco Porphyry Copper Deposit, Central Chile: Implications of an Integrated U-Pb and $^{40}Ar/^{39}Ar$ Database. *Econ Geol* **2005,** *100*(5): 905–934. https.//doi.or/10.2113/gsecongeo.100.5.905

31 Instituto de Investigaciones Geológicas (Chile), Thiele R.; Cubillos E. Hoja Santiago, Región Metropolitana: carta geológica de Chile escala 1:250.000. Instituto de Investigaciones Geológicas, **1980.**

32 Stambuck V.; Blondel J.; Serrano L. Geología del Yacimiento Río Blanco. *III Congr Geol Chileno Actas* **1982**, 419–442.

33 Toro J.C.; Ortúzar J.; Zamorano J.; Cuadra P.; Juan H.; Spröhnle C. Protracted Magmatic-Hydrothermal History of the Río Blanco-Los Bronces District, Central Chile: Development of World's Greatest Known Concentration of Copper. *Soc Eco Geo Spc Pub* **2012,** *16*: 105-126. https://doi.org/10.5382/SP.16.05

34 Piquer J.; Skarmeta J.; Cooke D.R. Structural Evolution of the Río Blanco-Los Bronces District, Andes of Central Chile: Controls on Stratigraphy, Magmatism, and Mineralization. *Econ Geol* **2012,** 110: 1995-2023. https://doi.org/10.2113/econgeo.1108.1995

35 Salinero J. Eventos de Alteración y Mineralización en el Sector Río Blanco, Yacimiento Río Blanco, V Región, Chile. Undergraduate thesis. Santiago de Chile, *Universidad de Chile* **2004**

36 Xiong Y.; Wood S.A. Experimental quantification of hydrothermal solubility of platinum-group elements with special reference to porphyry copper environments. *Miner Petrol* **2000,** 68: 1–28.

37 Sullivan N.A.; Zajacz Z., Brenan J.M. The solubility od Pd and Au in hydrous intermediate silicate melts: The effect of oxygen fugacity and the addition of Cl and S. *Geochim Cosmochim Ac* **2018,** 231: 15-29. https://doi.org/10.1016/j.gca.2018.03.019

38 Hanley J.J. The aqueous geochemistry of the platinum-group elements (PGE) in surficial, low-T Hydrothermal and High-T magmatic-hydrothermal environments. In: Mungall JE (ed) Exploration for Platinum-Group Elements Deposits. *Mineral Association Canada Short Course* **2005,** *35*: 35–56

39 Sillitoe R.H. Porphyry Copper Systems. *Econ Geol* **2010,** *105*: 3–41. https://doi.org/10.2113/gsecongeo.105.1.3

40 Kouzmanov K.; Pokrovski G.S. Hydrotermal controls on metal distribution in Porphyry Cu(-Mo-Au) Systems. *Soc Eco Geo Spc Pub* **2012,** *16: 573-618*

41 McFall K.; Roberts S.; Naden J.; Wilkinson C.; Wilkinson J.; Boyce A. Hydrothermal transport of PGEs in porphyry systems- a fluid history of the Skouries Cu-Au (PGE) porphyry deposit. *Appl Earth Sci* **2017,** 126: 79-80. https://doi.org/10.1080/03717453.2017.1306277